Supplementary Materials

Supplementary Notes
1. Linear-strain kinematics and statics
2. Discrete algorithm
3. Control with inverse statics

Supplementary Figures
Supplementary Figure 1: Stiffness distribution and contribution of homogeneous and helicoids cylinders.
Supplementary Figure 2: FEM Simulation of architectured structures with varied helical angles.
Supplementary Figure 3: FEM Simulation of architectured structures with varied helicoid numbers
Supplementary Figure 4: The mapping from helix strucutre to wave structure.
Supplementary Figure 5: The sensitivity and compliance analysis at Z axis.
Supplementary Figure 6: The sensitivity and compliance analysis at XY axis.
Supplementary Figure 7: The workspace reach-ability, sensitivity and compliance analysis of couple-tendon manipulator.

Supplementary Table
Supplementary Table 1: Precision of trajectory planning.

Supplementary Movies
Supplementary Movie 1: Trajectory planning simulation based on inverse statics.
Supplementary Movie 2: Trajectory planning simulation based on inverse statics.
Supplementary Movie 3: Robot-human tomato sorting.
Supplementary Movie 4: Robot-human fondue.

1. Supplementary Notes

1.1. Linear-strain kinematics and statics.

Assuming, the manipulator could be divided into N segments. To include the shear and torsion deformation, the general coordinates of the segment i, q_i was defined as below:

$$\begin{aligned} q_i &= [\gamma^0_{\mathrm{x},i}, \gamma^0_{\mathrm{y},i}, \varepsilon^0_{\mathrm{z},i}, k^0_{\mathrm{x},i}, k^0_{\mathrm{y},i}, \tau^0_{\mathrm{z},i}, \gamma^1_{\mathrm{x},i}, \gamma^1_{\mathrm{y},i}, \varepsilon^1_{\mathrm{z},i}, , k^1_{\mathrm{x},i}, k^1_{\mathrm{y},i}, \tau^1_{\mathrm{z},i}]^T \\ &= [\mathbf{u}^0_i, \mathbf{v}^0_i, \mathbf{u}^1_i, \mathbf{v}^1_i]^T, \\ &\text{with} \quad \mathbf{u}^0_i = [\gamma^0_{\mathrm{x},i}, \gamma^0_{\mathrm{y},i}, \varepsilon^0_{\mathrm{z},i}]^T,\ \mathbf{v}^0_i = [k^0_{\mathrm{x},i}, k^0_{\mathrm{y},i}, \tau^0_{\mathrm{z},i}]^T,\ \mathbf{u}^1_i = [\gamma^1_{\mathrm{x},i}, \gamma^1_{\mathrm{y},i}, \varepsilon^1_{\mathrm{z},i}]^T, \\ &\mathbf{v}^1_i = [k^1_{\mathrm{x},i}, k^1_{\mathrm{y},i}, \tau^1_{\mathrm{z},i},]^T,\ i = 1 \ldots N, \end{aligned} \tag{1}$$

$\gamma^0_{\mathrm{x},i}/\gamma^1_{\mathrm{x},i}$: the nominal z-y plane shear strain at the start/end point of the segment i,
$\gamma^0_{\mathrm{y},i}/\gamma^1_{\mathrm{y},i}$: the nominal z-z plane shear strain at the start point of the segment i,
$\varepsilon^0_{\mathrm{z},i}/\varepsilon^1_{\mathrm{z},i}$: the nominal z axial strain at the start point of the segment i,
$k^0_{\mathrm{x},i}/k^1_{\mathrm{x},i}$: the nominal x axis bending curvature at the start/end point of the segment i,
$k^0_{\mathrm{y},i}/k^1_{\mathrm{y},i}$: the nominal y axis bending curvature at the start/end point of the segment i,
$\tau^0_{\mathrm{z},i}/\tau^1_{\mathrm{z},i}$: the nominal z axis torsion rate at the start/end point of the segment i,
$\mathbf{u}^0_i/\mathbf{u}^1_i$: the strain vector related to the internal forces at the start/end point of the segment i,
$\mathbf{v}^0_i/\mathbf{v}^1_i$: the strain vector to the internal moments at the start/end point of the segment i.
Then the general coordinates of the manipulator can be expressed as:

$$Q = [q_1, \ldots, q_N]. \tag{2}$$

At a point along the centre line of the segment i, its general strains can be expressed as below:

$$\begin{aligned} q_{s,i}(s) &= (1-s)\left[\mathbf{u}^{0\,T}_i, \mathbf{v}^{0\,T}_i\right]^T + s\left[\mathbf{u}^{1\,T}_i, \mathbf{v}^{1\,T}_i\right]^T \\ &= \left[\gamma^s_{\mathrm{x},i}, \gamma^s_{\mathrm{y},i}, \varepsilon^s_{\mathrm{z},i}, k^s_{\mathrm{x},i}, k^s_{\mathrm{y},i}, \tau^s_{\mathrm{z},i}\right]^T = \left[\mathbf{u}^{s\,T}_i, \mathbf{v}^{s\,T}_i\right]^T \end{aligned} \tag{3}$$

where s is the nominal arc length coordinate $s \in [0,\ 1]$. The centre line configuration of the segment i can be calculated by integrating the following differential equations [49]:

$$\widetilde{\xi_{s,i}} = \begin{bmatrix} \widehat{\mathbf{v}_i^s} & \mathbf{u}_i^s + [0,0,1]^T \\ 0_{1\times 3} & 1 \end{bmatrix} \qquad (4)$$
$$g_{s,i}{}' = g_{s,i}\widetilde{\xi_{s,i}}$$

where $\widetilde{\xi_{s,i}}$ is the strain twist vector, the $'$ denotes a first derivative with respect to the nominal arc length s, and the $\hat{}$ symbol denotes mapping from R3 to so(3). And the solution of centre line, $g_{s,i}$, is an infinite series of the exponential, and only can be expressed in a compact way under some special situation such as with constant-strain.

Considering the torsion and shear stiffness of the manipulator in this work is much higher than bending and axial stiffness, it can be assumed that there is only bending and axial deformation existing with the manipulator body. Thus Eq. S(1), S(3) and can be rewritten as:

$$q_i = [k_{\mathrm{x},i}^0, k_{\mathrm{y},i}^0, \varepsilon_{\mathrm{z},i}^0, k_{\mathrm{x},i}^1, k_{\mathrm{y},i}^1, \varepsilon_{\mathrm{z},i}^1]^T = [\mathbf{q}_i^{0\,T}, \mathbf{q}_i^{1\,T}]^T, \qquad (5)$$
$$\text{with } q_i^0 = [k_{\mathrm{x},i}^0, k_{\mathrm{y},i}^0, \varepsilon_{\mathrm{z},i}^0]^T,\ q_i^1 = [k_{\mathrm{x},i}^1, k_{\mathrm{y},i}^1, \varepsilon_{\mathrm{z},i}^1]^T$$

$$q_{s,i}(s) = (1-s)\,\mathbf{q}_i^0 + s\mathbf{q}_i^1 \qquad (6)$$

Since the torsion and shear ratio of the manipulator were assumed as zero, the Eq. (4) can be rewritten as:

$$P_{s,i}{}' = R_{s,i}[0,0,1+\varepsilon_{\mathrm{z},i}^s]^T, \qquad (7)$$
$$R_{s,i}{}' = R_{s,i}([k_{\mathrm{x},i}^s, k_{\mathrm{y},i}^s, 0]^T)^\wedge$$

Its quasi-static state can be solve by a pseudo dynamic equation when $\dot{q}, \ddot{q} \approx 0$, as:

$$G(q_{s,i}) + D\ \dot{q}_{s,i} + FM_{s,i}(s) = FM_{\mathrm{ext}}(q_{s,i}) + FM_{\mathrm{T},i} \qquad (8)$$
$$\text{with}\quad FM_{s,i} = \begin{bmatrix} M_{\mathrm{x},i}^s \\ M_{\mathrm{y},i}^s \\ F_{\mathrm{z},i}^s \end{bmatrix} = K_{\mathrm{stiff}}q_{s,i}(s), \quad \text{and} \quad K_{\mathrm{stiff}} = \begin{bmatrix} K_{\mathrm{bend}} & 0 & 0 \\ 0 & K_{\mathrm{bend}} & 0 \\ 0 & 0 & K_{\mathrm{axial}} \end{bmatrix},$$

where G is the gravitational force, D is the damping matrix, K_{stiff} is the stiffness matrix, $FM_{s,i}$ is the internal load from stiffness, FM_{ext} is the external load, and FM_{T}, is the tendon actuation load. $M_{\mathrm{x},i}^s$, $M_{\mathrm{y},i}^s$ and $F_{\mathrm{z},i}^s$ are moment/force components on x, y and z axis. K_{bend}, is the bending stiffness and K_{axial}, is the axial stiffness.

The relationship between tendon lengths $L_i = [L_{1,i}, L_{2,i}, L_{3,i}]$ and general coordinates q_i of the segment i can be draw as follows.

$$q_{\mathrm{av},i} = \int_0^1 q_{s,i}ds = \left[k_{\mathrm{x},i}^{\mathrm{av}}, k_{\mathrm{y},i}^{\mathrm{av}}, \varepsilon_{\mathrm{z},i}^{\mathrm{av}}\right]^T = \left(\left[k_{\mathrm{x},i}^0, k_{\mathrm{y},i}^0, \varepsilon_{\mathrm{z},i}^0\right]^T + \left[k_{\mathrm{x},i}^1, k_{\mathrm{y},i}^1, \varepsilon_{\mathrm{z},i}^1\right]^T\right)/2 \qquad (9)$$

where $q_{av,i}$ is the averaged strain vector.

The position of three tendon at the section for the segment i can be written as:

$$P_{\mathrm{tendon},j} = R_i[\cos(\theta_j), \sin(\theta_j)], j = 1,2,3, \qquad (10)$$

where R_i is the distance from tendons to the center of segment i (could be different from the initial value), and θ_j is the orientation angle of tendon j.

Then, the variation of tendon lengths can be derived as:

$$\Delta TL_i = T_{\mathrm{Def2\Delta TL},i}\ q_{\mathrm{av},i} \qquad (11)$$
$$T_{\mathrm{Def2\Delta TL},i} = \begin{bmatrix} R_i\sin(\theta_1) & -R_i\cos(\theta_1) & 1 \\ R_i\sin(\theta_2) & -R_i\cos(\theta_2) & 1 \\ R_i\sin(\theta_3) & -R_i\cos(\theta_3) & 1 \end{bmatrix}.$$

1.2. **Discrete algorithm.**

Due to the variable curvatures and strains, it is difficult to get an close-form expression of the robot configuration. Even though numerical integration could be involved to obtain a numerical solution with trade of calculation efficiency, its continuous form may be not be appropriate for some robots with un-deformable regions. The PCC model has been investigated intensively, and works well in some situations with low gravity effect, low load bearing and constant stiffness. But when the gravity effect, bearing loads or stiffness variation are non-negligible, PCC would have to pay a much higher cost to reconstruct the configuration of robot body with more discrete elements.

Here, a discrete algorithm was proposed to facilitate the calculation by projecting the high order solution space of discrete constant strain elements to the low-order subspace solution space of the linear strain segment. And due to the constant strain, the configuration of elements can be expressed in a compact way [49]. When the shear strains $\gamma_{\mathrm{x}}, \gamma_{\mathrm{y}} = 0$, its configuration will be a helical curve [50]. When $\gamma_{\mathrm{x}}, \gamma_{\mathrm{y}} = 0$ and torsion rate $\tau_{\mathrm{z}} = 0$, its configuration will be a constant curvature arc as that in PCC model, which are easier for computation. But by reducing the dimension of PCC model and keeping the variable curvature and strain of robot body, the subspace projection (SP) method can achieve higher calculation efficiency and reconstruct the robot deformation reasonably.

For each segment i, it can be divided into N elements. Assuming the curvature and strain of each element k is constant, the force balancing equations of each element can be derived as:

$$q_{\mathrm{e},i}^{k} = q_i\left(s_k\right) = \left(1 - s_k\right)\left[k_{\mathrm{x},i}^{0}, k_{\mathrm{y},i}^{0}, \varepsilon_{\mathrm{z},i}^{0}\right]^T + s_k\ \left[k_{\mathrm{x},i}^{1}, k_{\mathrm{y},i}^{1}, \varepsilon_{\mathrm{z},i}^{1}\right]^T = \left[k_{\mathrm{x},i}^{k}, k_{\mathrm{y},i}^{k}, \varepsilon_{\mathrm{z},i}^{k}\right]^T \tag{12}$$

$$q_{\mathrm{e},i} = \left[{q_{\mathrm{e},i}^{1}}^{T}, \ldots, {q_{\mathrm{e},i}^{N}}^{T}\right]^T = \begin{bmatrix} \vdots & \vdots & \vdots & \vdots & \vdots & \vdots \\ 1-s_k & 0 & 0 & s_k & 0 & 0 \\ 0 & 1-s_k & 0 & 0 & s_k & 0_1 \\ 0 & 0 & 1-s_k & 0 & 0 & s_k \\ \vdots & \vdots & \vdots & \vdots & \vdots & \vdots \end{bmatrix} \begin{bmatrix} k_{\mathrm{x},i}^{0} \\ k_{\mathrm{y},i}^{0} \\ \varepsilon_{\mathrm{z},i}^{0} \\ k_{\mathrm{x},i}^{1} \\ k_{\mathrm{y},i}^{1} \\ \varepsilon_{\mathrm{z},i}^{1} \end{bmatrix} = T_{\mathrm{Q2q}} q_i \tag{13}$$

Assuming $q_{\mathrm{e},i}$ is static solution of the segment i, there may be no solution of Q for Eq. S(8), but a projected solution $Q_{\mathrm{p},i}$ can be derived as below to obtain least square solution of $q_{\mathrm{e},i}$.

$$Q_{\mathrm{p},i} = \left({T_{\mathrm{Q2q}}}' T_{\mathrm{Q2q}}\right)^{-1} {T_{\mathrm{Q2q}}}' q_{\mathrm{e},i} \tag{14}$$

And here, instead of solving the static solution of q_e directly, Eq. S(8) was only utilized to calculate the iterated variation dQ.

$$\begin{aligned} \dot{q}_{\mathrm{e},i}^{k} &= D^{-1}(FM_{\mathrm{ext},i}^{k}(q_{\mathrm{e},i}^{k}) + FM_{\mathrm{T},i}^{k} - K_{\mathrm{stiff}}, q_{\mathrm{e},i}^{k} - G(q_{\mathrm{e},i}^{k})) \\ \dot{Q}_{\mathrm{p},i} &= (T_{\mathrm{Q2q}}' T_{\mathrm{Q2q}})^{-1} T_{\mathrm{Q2q}}' \dot{q}_{\mathrm{e},i}^{k} \end{aligned} \tag{15}$$

By assuming $D = c_{\mathrm{damp}} K_{\mathrm{stiff}}$, and setting $t_{step} = 1$, the Q in next time step $t+1$, $Q\left(t+1\right)$, can be written as below.

$$\begin{aligned} &dQ_{\mathrm{p},i} = (T_{\mathrm{Q2q}}' T_{\mathrm{Q2q}},)^{-1} T_{\mathrm{Q2q}}' {K_{\mathrm{stiff}}}^{-1} \left[FM_{\mathrm{ext},i}^{k}(q_{\mathrm{e},i}^{k}) + FM_{\mathrm{T},i}^{k} - K_{\mathrm{stiff}} q_{\mathrm{e},i}^{k} - G(q_{\mathrm{e},i}^{k})\right] / c_{\mathrm{damp}} \\ &Q\left(t+1\right) = Q\left(t\right) + dQ_{\mathrm{p}}, \\ &Q_{\mathrm{static}} = \lim_{t \to \infty} Q\left(t\right) \end{aligned} \tag{16}$$

1.3. **Control with inverse statics.**

To get to the target state, the tension forces of 9 tendons were chosen as control parameters to approach the target state. The evaluation indexes of error between the present state S_{pre} and target S_{target} state are defined as below.

$$\begin{aligned} &Error = \begin{bmatrix} P_{\mathrm{pre}} \\ \left(R_{\mathrm{pre}}^{-1} R_{\mathrm{target}} - R_{\mathrm{target}}^{T} R_{\mathrm{pre}}^{-T}\right)^{\vee} \end{bmatrix}, \\ &with \quad S_{\mathrm{pre}} = \begin{bmatrix} R_{\mathrm{pre}} & P_{\mathrm{pre}} \\ 0_{1\times 3} & 1 \end{bmatrix}, \quad S_{\mathrm{target}} = \begin{bmatrix} R_{\mathrm{target}} & P_{\mathrm{target}} \\ 0_{1\times 3} & 1 \end{bmatrix}. \end{aligned} \tag{17}$$

the $\vee$ symbol denotes inverse mapping of $\hat{}$, i.e. $\left(\hat{x}\right)^{\vee} = x$. Thus the Jacobian matrix $J(F_{\mathrm{T}},)$ between the tendon forces TF and $Error$ can be expressed as below:

$$J\left(F_{\mathrm{T}},\right) = \frac{\partial Error}{\partial F_{\mathrm{T}},} = J_{6\times 9} \tag{18}$$

where $TF_{1,j} = F_{T,j}$, $TF_{2,j} = TF_{3,j} = F_{T,j+3}$, $TF_{4,j} = TF_{5,j} = F_{T,j+6}$, $F_{\mathrm{T}}, = [F_{T,1}, \ldots, \ F_{T,9}]'$, $j = 1, 2, 3$. Then the Eq. (19) can be derived.

$$J_{6\times 9} dF_{\mathrm{T}}, = -Error \tag{19}$$

Since the manipulator is redundant, there are infinite solutions for Eq.(19) in theory, but here the least norm solution was introduced to get closest solution of F_{T}, from the present state as:

$$dF_{\mathrm{T}}, = \mathrm{pinv}\,(J_{6\times 9})\, Error_{6\times 1} \tag{20}$$

$$F_{\mathrm{T}}^{k+1} = F_{\mathrm{T}}^{k} + \lambda dF_{\mathrm{T}}, \lambda > 0 \tag{21}$$

where λ is step length scaling factor.

2. Supplement figures

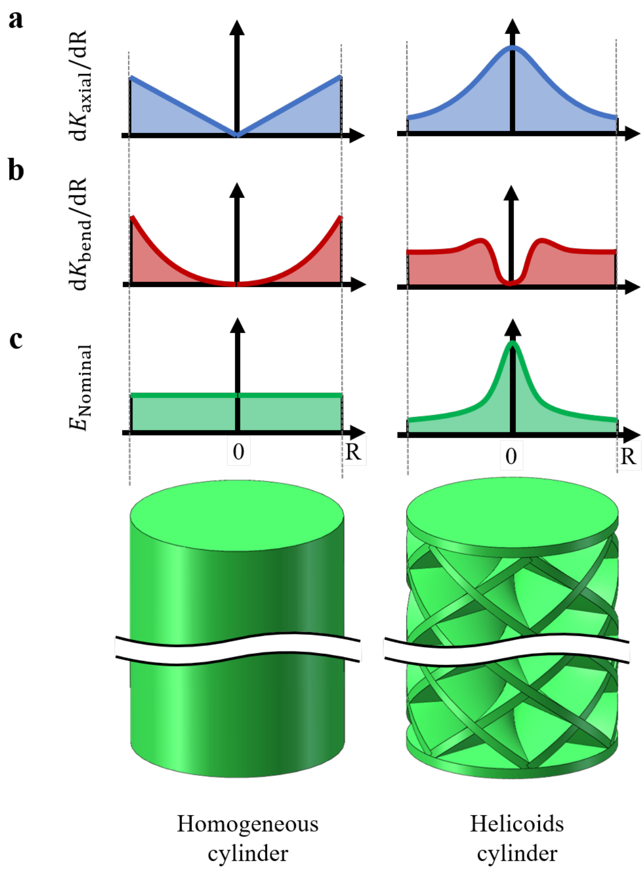

Supplementary Figure 1. Stiffness distribution and contribution of homogeneous (left) and helicoids (right) cylinders. (a) The contribution to axial stiffness, dK_{axial}/dR, from the material at different radius R. (b) The contribution to bending stiffness, dK_{bend}/dR, from the material at different radius R. (c) The local axial nominal modulus, E_{nominal}, at different radius R.

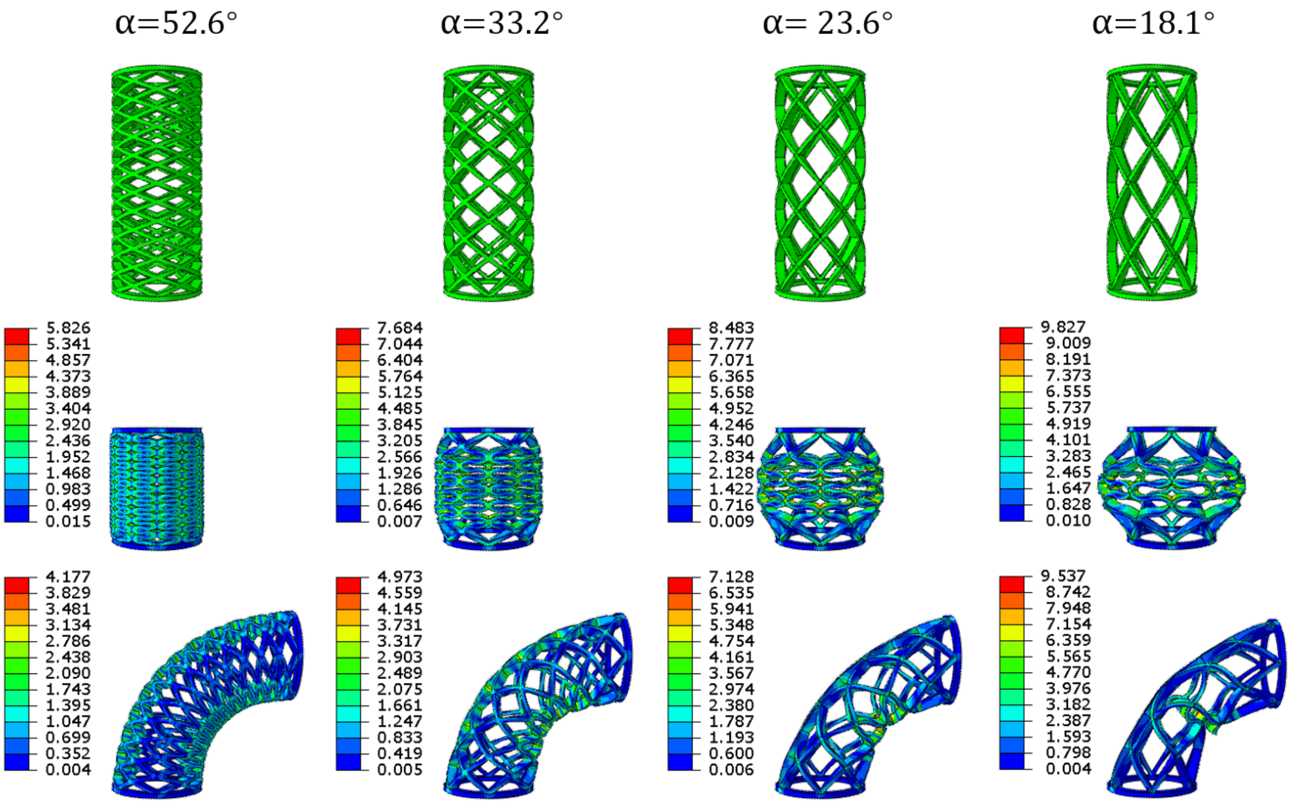

Supplementary Figure 2. FEM Simulation of architectured structures with varied helical angles

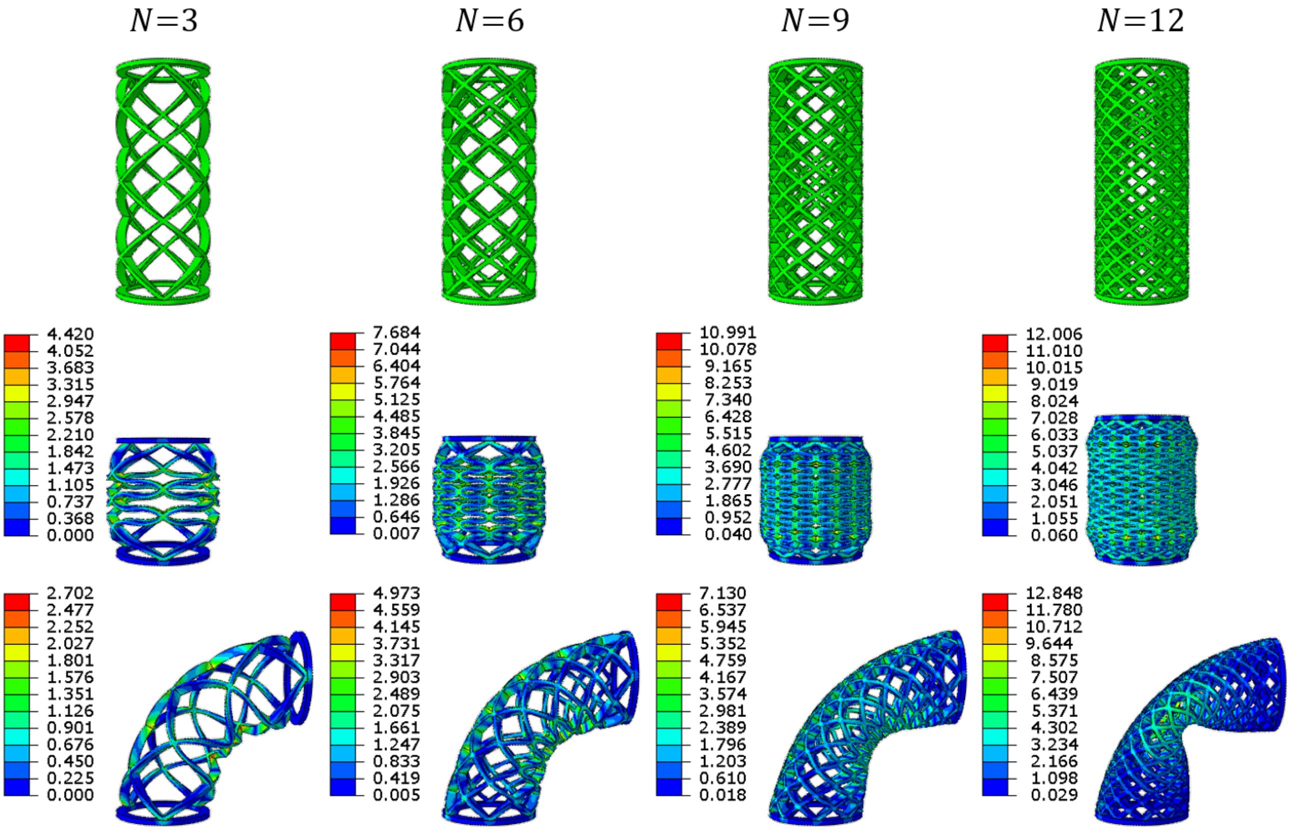

Supplementary Figure 3. FEM Simulation of architectured structures with varied helicoid numbers

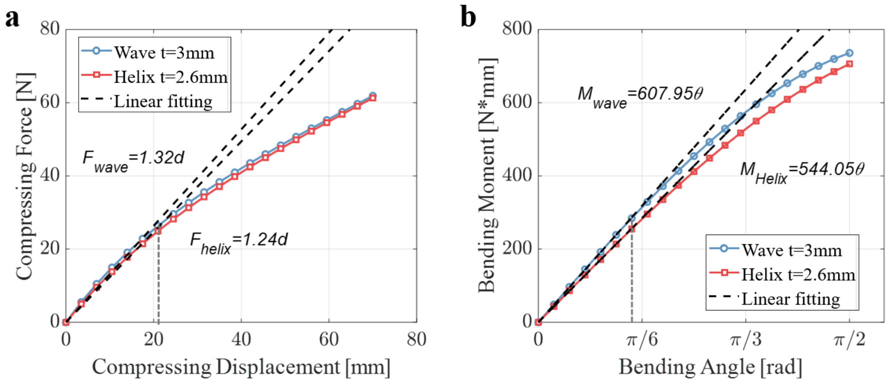

Supplementary Figure 4. The mapping from helix strucutre to wave structure. The wave structure was involved to reduce the stress concentration without changing much of its property

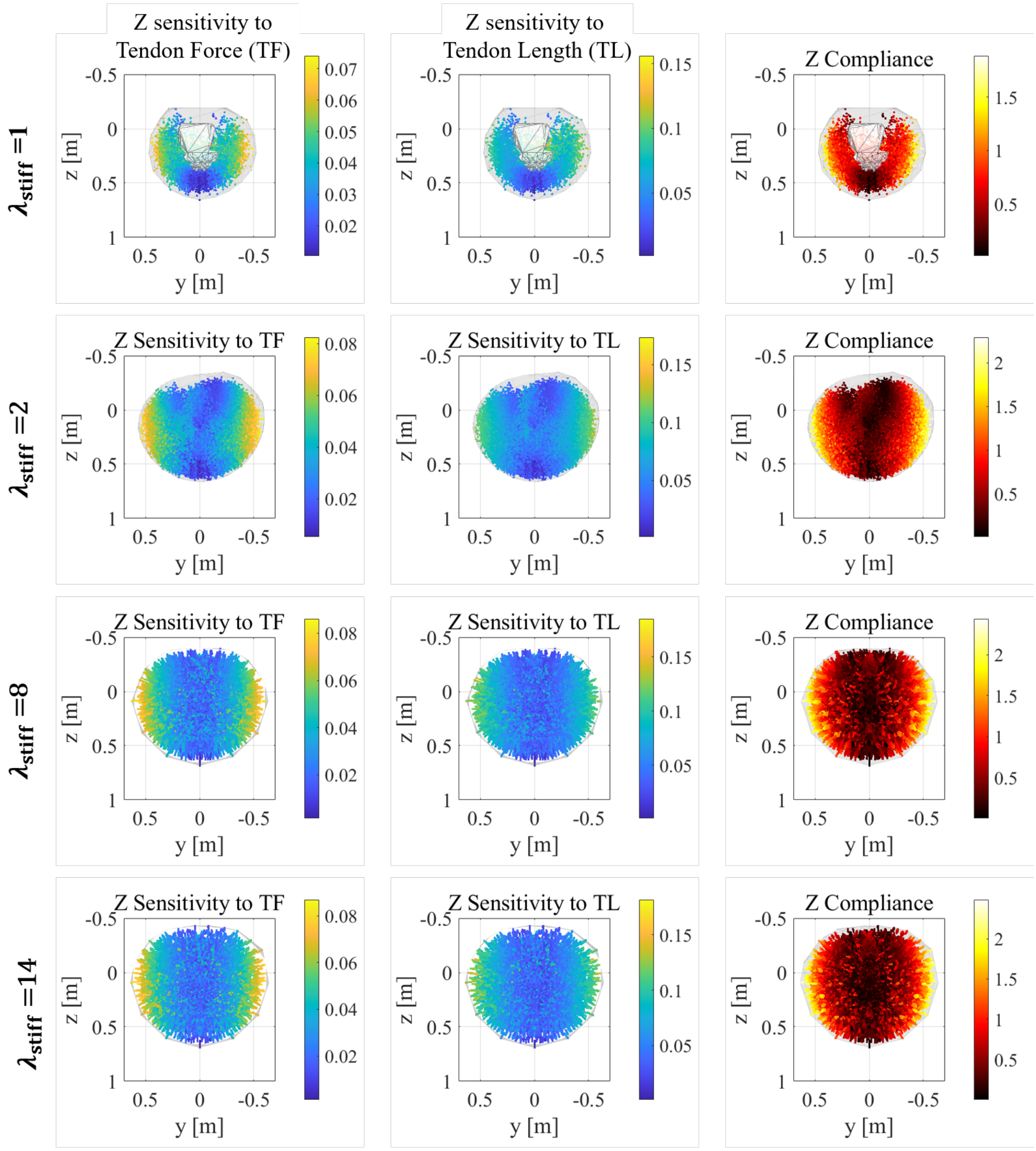

SUPPLEMENTARY FIGURE 5. The sensitivity and compliance analysis at Z axis

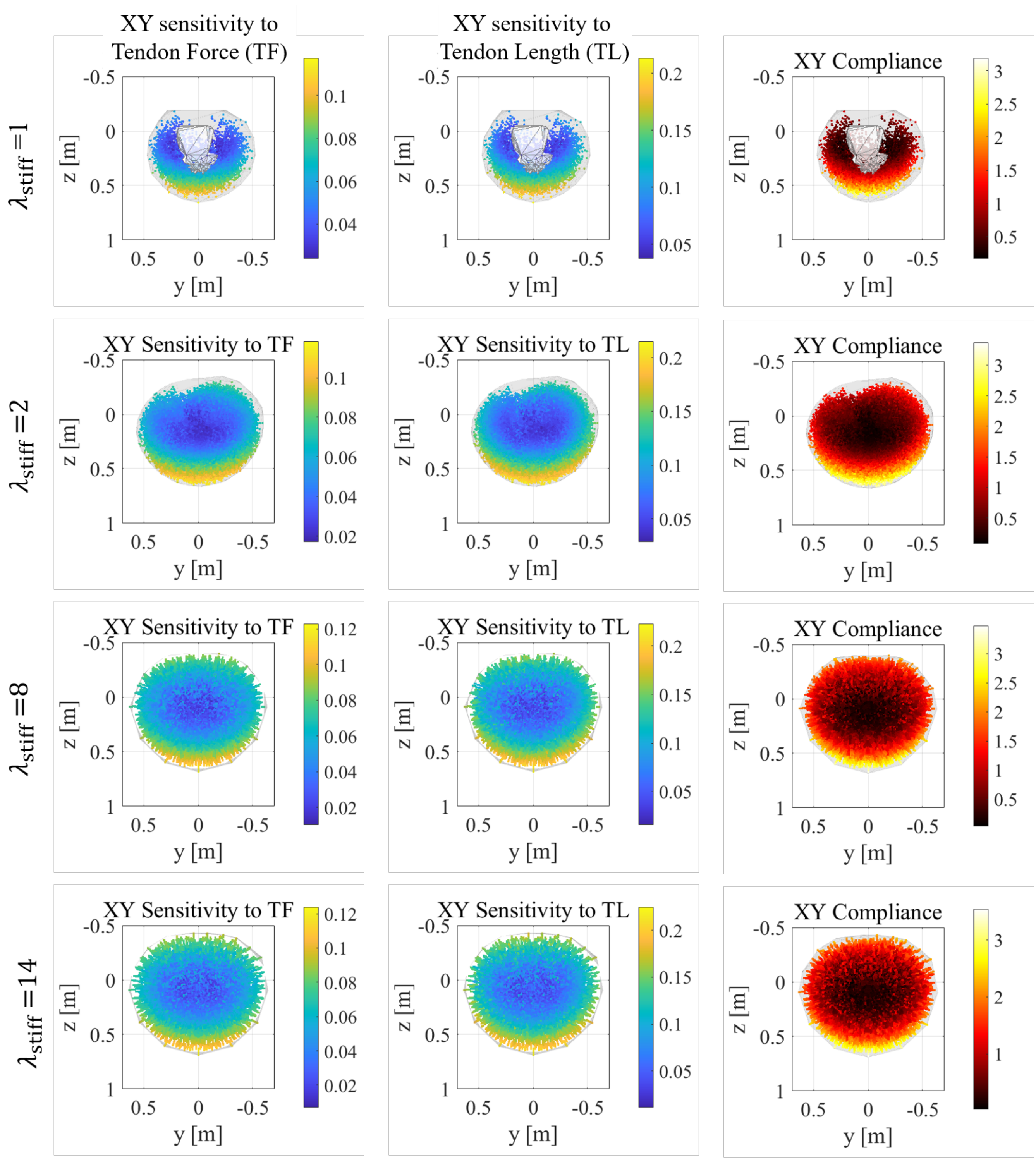

SUPPLEMENTARY FIGURE 6. The sensitivity and compliance analysis at XY axis

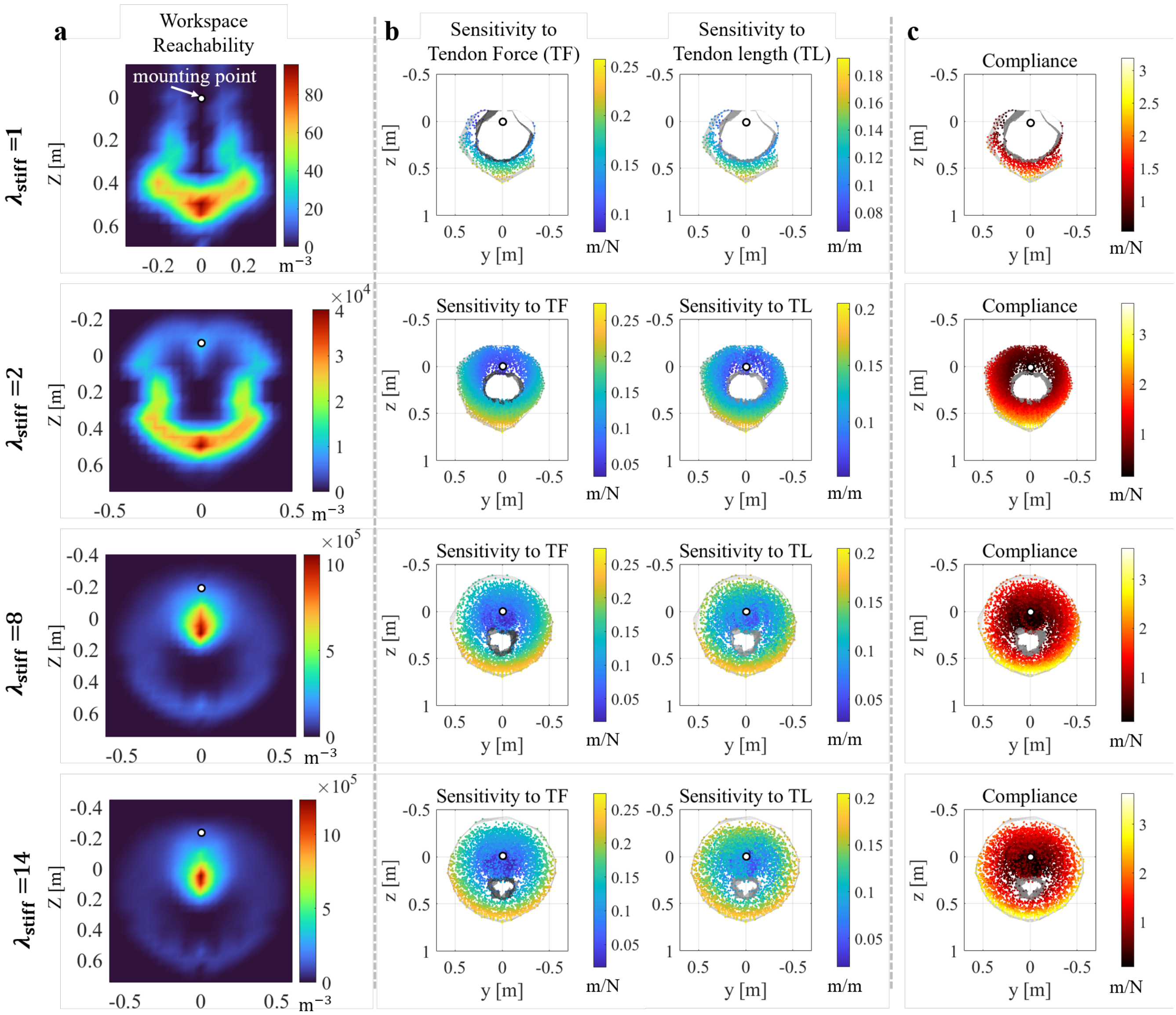

SUPPLEMENTARY FIGURE 7. The workspace reach-ability, sensitivity and compliance analysis of couple-tendon manipulator

3. SUPPLEMENT TABLES

We report here the precision achieved with the manipulator for the trajectories shown in Table 1:

Supplementary Table 1. Precision of trajectory planning

	Position XYZ (cm)	Scale (cm), (configuration)	Trajectory RMSE error (cm)			Centre position offset (cm)		
			XY	Z	Overall	XY	Z	Overall
Circle 1	0 , 0 ,70	60,(D)	3.1	1.7	3.5	1.2	1.6	2.1
Circle 2	0 , 0 ,50	60,(D)	2.8	1.9	3.4	2.5	–0.3	2.5
Square 1	0 , 0 ,60	40,(L,sym)	4.5	1.5	4.8	4.2	-0.9	4.3
Square 2	0 , 0 ,60	40,(L,mono)	4.8	2.7	5.5	4.4	-2.4	5.0
Null-space 1	0 , 0 ,70	-	2.7	1.0	2.9	2.0	-0.6	2.1
Null-space 2	0 ,-10,70	-	3.2	2.2	3.9	1.7	-2.1	2.7
Null-space 3	10, 0,70	-	4.7	1.6	5.0	3.9	-1.5	4.1

* L: length of the square's side, sym: symmetrical, mono: mono-directional.